Enhanced performance of single and double junction plastic solar cells

Moet, Date Jan David

Chapter 6

Enhanced efficiency in double-junction polymer:fullerene solar cells

Abstract

Realizing a considerable improvement in the performance of polymer photovoltaic devices seems to require a reduction of the absorber's bandgap, which enables an enhanced spectral overlap of absorption and irradiance. Ultimately, such small-bandgap materials could be used in tandem solar cells containing two subcells with complementary absorption spectra. However, realizing more efficient solar cells with tandem structures is not restricted to the use of new materials. This chapter deals with the role of device architecture in the optimization of an existing bulk heterojunction system. It is demonstrated that the optimum thickness of the 4%-efficient high-molecular-weight PF10TBT:PCBM devices discussed in Chapter 2 is just 80 nm. Films that thin absorb only half of the photons available in the absorption bandwidth. The thickness limitation arises from electronic losses in thicker cells, which are subject to the effects of space charge and recombination. In the previous chapter, we have presented a high-work-function middle electrode that is compatible with PF10TBT in solution-processed tandem devices. Here, we demonstrate with simulations and experiments that using such a double-junction device architecture is a very effective way to decouple the optical and electronic limitations in PF10TBT:PCBM solar cells. The measured power conversion efficiency of tandem cells in which two thin subcells are integrated amounts to 4.5%, which is 13% higher (relative) than that of an optimized single-junction cell.

Published as:
D. J. D. Moet, P. de Bruyn, J. D. Kotlarski, and P. W. M. Blom, Org. Electron. **11**, 1821 (2010).

6.1 Introduction

The power conversion efficiency of thin-film polymer photovoltaic devices is mainly limited by a relatively low photocurrent as a result of a high bandgap and narrow absorption bandwidth. An enhancement in performance therefore primarily requires that more photons are collected. The most direct way to increase absorption is increasing the thickness of the photoactive layer. However, in many polymer:fullerene systems the combined effects of charge carrier recombination and the formation of space charge reduce the fill factor and consequently the overall device efficiency of thick cells.[1] It has been suggested that the photocurrent of thin polymer cells can be increased by introducing an optical spacer that enhances light absorption by redistributing the optical electric field.[2,3] However, the spacer effect is only beneficial if the BHJ film thickness does not coincide with a local maximum of optical power dissipation.[4] Alternatively, the optical properties of the photoactive materials can be tuned. Promising results have been reported for solar cells in which narrow bandgap polymers were introduced in order to absorb low-energy photons.[5–7] The electron-accepting material can be modified as well: substitution of PCBM with its more strongly absorbing C_{70}-analogue generally results in a larger contribution to the photocurrent.[8] A further improvement of the spectral overlap with the solar spectrum can be realized by incorporation of multiple heterojunctions with complementary absorption spectra in a tandem solar cell.[9–11]

This chapter presents an alternative approach to improve the performance of thin-film polymer photovoltaics using a tandem architecture. Instead of relying on a broader spectral coverage of the solar spectrum using small-bandgap materials, it enables enhanced light harvesting by the available absorber material. The working principle is generic for bulk heterojunctions of which the optimum layer thickness is limited by electronic limitations. As a model system, we use polymer solar cells based on PF10TBT and PCBM with a power conversion efficiency of 4%. The efficiency is enhanced to 4.5% by combining two optimized PF10TBT:PCBM solar cells in one double-junction device, without any change to the constituents of the photoactive layer. The approach concurrently utilizes the enhanced absorption of thick films and the superior electronic performance of thin films.

6.2 Single-junction PF10TBT:PCBM solar cells

The efficiency of PF10TBT:PCBM solar cells is known to increase with the molecular weight of the polymer. As discussed in Chapter 2, this is caused by a reduced recombination rate of bound electron–hole pairs at high molecular weights, which leads to more efficient generation of free charges.[12] Therefore, the solar cells studied here are based on bulk heterojunctions of PCBM and high-molecular-weight PF10TBT. The donor–acceptor

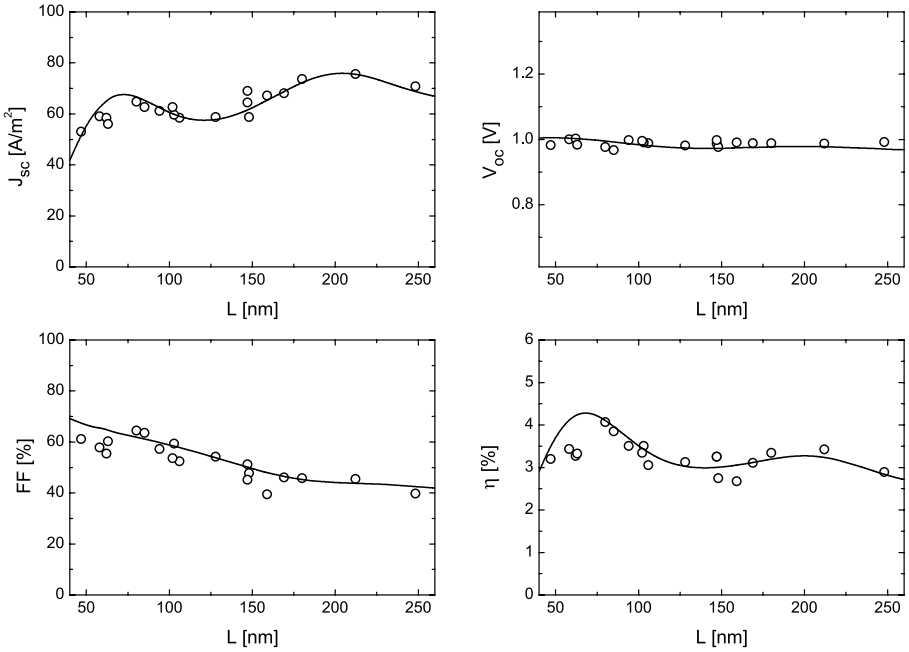

Figure 6.1: Experimental photovoltaic data of PF10TBT:PCBM solar cells with varying active layer thickness (circles) and the results of combined optoelectronic simulations (solid lines).

weight ratio was fixed to the optimal 1:4 and all devices were processed from hot chlorobenzene solutions.

The variation of short-circuit current density, open-circuit voltage, fill factor and power conversion efficiency of PF10TBT:PCBM solar cells with photoactive layer thickness are displayed in Figure 6.1. Each data point represents the average outcome for three or more devices. The values of J_{sc} and η were corrected for spectral mismatch of the lamp with the solar spectrum (see Section 6.5). Noticeable is the oscillatory behavior of J_{sc}, characterized by maxima at $L = 80$ nm and $L = 210$ nm. Thicker cells clearly absorb more light as J_{sc} is highest for $L > 150$ nm. However, since the open-circuit voltage is virtually independent of layer thickness and the fill factor strongly decreases with increasing L, the overall experimental η reaches its highest value of 4.0% already at $L = 80$ nm.

Next, we use combined optoelectronic modeling to gain insight in the major limitations of PF10TBT:PCBM solar cells of varying thickness. In order to describe the experimental results, we combine the optical and electronic models that were introduced in Section 1.5.

Optical simulations

As input for the optical model, the index of refraction n, extinction coefficient k and thickness of each layer in the device architecture are used. The optical constants were determined previously using variable-angle spectroscopic ellipsometry [12] and are given in Figure 2.2a. The light intensity $I(\lambda, x)$ is calculated for each wavelength and position inside the entire layer stack, taking into account the optical properties of each layer as well as the interference of light that is incident on the device (AM1.5G, 1000 W/m^2) with light that is reflected by the back electrode. The exciton generation rate at each position in the polymer:fullerene layer is given by the convolution of the local spectral photon flux and the absorption spectrum of the active layer. [13] In the calculation the relevant wavelength range is discretized at exponentially equidistant values λ_i and the integral is consequently replaced by a summation:

$$G(x) = \sum_i \frac{4\pi k(\lambda_i)}{hc} I(\lambda_i, x) \Delta\lambda_i. \tag{6.1}$$

$G(x)$ is the exciton generation rate at position x, h is Planck's constant, c is the speed of light and $I(\lambda_i, x)$ is the light intensity at wavelength λ_i and position x. The exciton generation profiles $G(x)$ are used below as an input for the electronic device model. A final integration of $G(x)$ over the position in the device gives the total generation rate G_{tot} of excitons inside the photoactive layer.

By definition, the amount of absorbed photons is equal to the amount of photogenerated excitons G_{tot}. For the AM1.5G reference spectrum, the number of incident photons with wavelengths within the effective absorption bandwidth of PF10TBT:PCBM layers, i.e., $300 < \lambda < 650$ nm, is $N_{\mathrm{ph}} = 1.05 \times 10^{21}$ m^{-2}s^{-1}. A measure of the absorption efficiency is now given by the ratio of G_{tot} to N_{ph}, which is plotted versus layer thickness in Figure

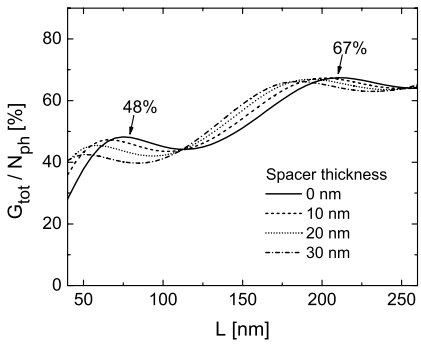

Figure 6.2: Ratio of photogenerated excitons G_{tot} to the amount of photons N_{ph} with $300 < \lambda < 650$ nm as a function of layer thickness. The lines denote different optical spacer thicknesses as indicated in the legend.

6.2. At $L = 80$ nm, which is the point of the first maximum of the experimental J_{sc}, only 48% of the available photons are absorbed. Poor light absorption thus strongly limits the current these thin PF10TBT:PCBM solar cells can produce. As expected, this conclusion is not altered by the introduction of an optical spacer in the form of a thin ZnO layer between the active layer and the cathode, since the incoupling of light is already optimal, giving a local maximum of the dissipated optical power at $L = 80$ nm. At the other local maximum of the experimental short-circuit current density, $L = 210$ nm, two-thirds of the available photons are absorbed. This shows that the available light can be used more efficiently in order to increase cell performance, without reducing the bandgap of the polymer.

Electronic simulations

In polymer:fullerene solar cells, each of the processes involved in photocurrent generation generally introduces electrical losses that reduce the amount of extracted charges. The cumulative effect of these losses at short-circuit conditions is represented in the internal quantum efficiency, defined as the number of electrons in an external circuit per absorbed photon, or $\mathrm{IQE} = J_{sc}/qG_{tot}$, where q is the elementary charge. The IQE can thus directly be determined from the measured J_{sc} (Figure 6.1) and calculated G_{tot} (Figure 6.2). In Figure 6.3, the resulting IQE is plotted versus photoactive layer thickness. Approximately 80% of the absorbed photons contribute to the photocurrent in thin cells. For thicker layers this fraction decreases monotonically to around 70%, which is in good agreement with previously reported results.[14]

Next, the current–voltage characteristics are simulated for each L in the range of experimental layer thicknesses. Here we use again our numerical device model.[15] The exciton generation profiles obtained by optical modeling are used as an input for the electronic model. Since ultrafast electron transfer from the photoexcited polymer to PCBM is as-

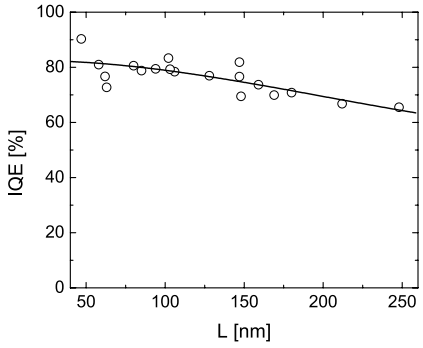

Figure 6.3: The internal quantum efficiency $\mathrm{IQE} = J_{sc}/qG_{tot}$ versus photoactive layer thickness. The line serves as a guide to the eye.

sumed to occur with unity quantum yield, the model assumes that each exciton generates a bound e–h pair at an interface of donor and acceptor molecules. In Figure 6.1, the results of the optoelectronic simulations are depicted by the solid lines. Clearly, the oscillations of the short-circuit current density and power conversion efficiency with thickness are reproduced, as well as the strongly decreasing fill factor. The values that were used for the parameters in the electronic model are in excellent agreement with those previously derived for high-molecular-weight PF10TBT:PCBM cells (see Ref. 12 and Chapter 2) and are summarized in Table 6.1. The simulations indicate an optimal thickness of around 70 nm, which is close to the experimental value of 80 nm. The ratio of the amount of excitons that are lost due to quenching at the electrodes to the total amount of photogenerated excitons is large in very thin cells. As this quenching effect is not incorporated in the model, the calculations slightly overestimate the fill factor and short-circuit current in thin cells and, consequently, the predicted value of the maximum η of 4.3% is somewhat higher than the optimal experimental value.

Based on the optical simulations, a relative increase of 40% in J_{sc} would be expected for a 210 nm thick cell compared to the 80 nm thick device. As can be seen in Figure 6.1, enhanced absorption in thicker cells does indeed enable the extraction of a higher current. However, limited by space charge effects and recombination, the short-circuit current at $L = 210$ nm is only 16% higher than that at $L = 80$ nm. The same limitation causes the fill factor to drop considerably, resulting in a reduction of η to 3.2%.

This clearly demonstrates that the increased absorption in thick cells is opposed by less favorable electronic properties. As a result, the processing window for optimized solar cells is limited to thin layers. In the following section, the interlocking of optics and electronics is reduced by using double-junction solar cells consisting of two optimized thin-layer devices.

Table 6.1: Overview of the model parameters used in the simulations.

Parameter	Symbol	Value
Effective bandgap	E_{gap}	1.37 eV
Electron mobility	μ_e	1×10^{-7} m^2/Vs
Hole mobility	μ_h	6×10^{-9} m^2/Vs
Effective density of states	N_c	2.5×10^{25} m^{-3}
Relative dielectric constant	ε_r	3.6
Initial bound pair distance	a	2.2 nm
Bound pair decay rate	k_f	5×10^5 s^{-1}

6.3 Double-junction solar cells

Multijunction solar cells are generally used to compensate for the relatively narrow absorption bandwidth of conjugated polymers. By inclusion of a second bulk heterojunction with a smaller optical bandgap, photon harvesting can be extended from the visible towards the near infrared. However, as discussed above, thin solar cells based on large-bandgap materials fail to absorb a lot of photons with sufficient energy. In the remainder of this chapter, we therefore choose to investigate the possibility to enhance absorption of these high-energy photons.

The photovoltaic properties of a multijunction solar cell depend on the method of interconnection of the subcells. The most practical approach is to use a series-connected multijunction, in which an increase in the amount of absorbed photons is utilized to deliver a higher voltage rather than a high current. Here, we employ the middle electrode made of ZnO nanoparticles and pH-modified PEDOT:PSS, which was developed by Gilot et al. [16] For practical reasons, the thicknesses of these layers are fixed to 20 and 30 nm, respectively.

Simulations

As a reference, we first take a step back to examine the exciton generation profiles of a thin and a thick device, as shown in the two left panels of Figure 6.4. Again we consider the layer thicknesses at the maxima of the experimental J_{sc} and η, i.e., $L = 80$ nm and $L = 210$ nm. The position x varies on the vertical axis and $x = 0$ corresponds to the interface of PEDOT:PSS with the photoactive layer, while the cathode is located at $x = L$. The light can thus be considered incident from the bottom of the figure. As expected, both profiles show excellent incoupling of the incident light. Furthermore, as discussed in Section 6.2, the ratio of the total exciton generation rates amounts to $G_{tot}^{thick}/G_{tot}^{thin} = 1.40$, which means that the thick cell absorbs 40% more photons than the thin one.

In the rightmost panel of Figure 6.4, the exciton generation profiles inside the two subcells of a double-junction device are plotted. As a one-to-one extension of the optimized single-layer cell, the tandem device is chosen to incorporate two thin PF10TBT:PCBM cells of 80 nm thickness. These are separated by a ZnO cathode (20 nm) for the front cell and *p*H-modified PEDOT:PSS anode (30 nm) for the back cell, which results in a total device thickness of 210 nm. It can be seen that the shape of the generation rate profile in the back cell is similar to the one of the single thin layer because it is closest to the reflective cathode. As expected the magnitude of $G(x)$ in the back cell is lower than in the single-layer thin cell due to optical interference effects and absorption in the front cell. However, in total the double-junction absorbs more photons, in fact nearly as much (96%) as the 210 nm thick single-layer device. In contrast, a single layer of 160 nm thickness absorbs only 81% of G_{tot}^{thick}. In other words, the double-junction device absorbs more photons per unit length

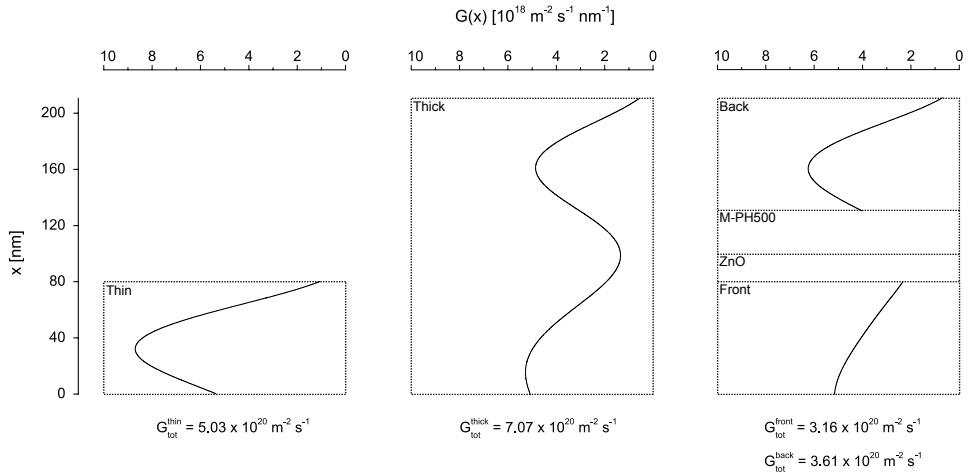

Figure 6.4: Calculated exciton generation rate profiles $G(x)$ as a function of the position x in a thin (left), a thick (middle) and a double-junction solar cell (right). The total integrated exciton generation rate G_{tot} for each profile is indicated in the relevant figure panel.

of photoactive material than thick single-layer cells due to the presence of the transparent middle electrode.

In order to predict the photovoltaic properties of the double-junction device, we consider the general properties of a series-connected tandem cell. First, since each subcell is as thick as the thin single-layer device and based on the same donor-acceptor system, it is reasoned that they will exhibit a similar IQE, FF and V_{oc}. Similarly, this also means that the FF of the double-junction device will be the same as the FF of the subcells whereas its V_{oc} will be twice as large. Of the two subcells in the particular double-junction device considered in Figure 6.4, the front cell produces the least amount of excitons ($G_{\mathrm{tot}}^{\mathrm{front}} < G_{\mathrm{tot}}^{\mathrm{back}}$). As the IQE is invariant, this subcell will be current-limiting under short-circuit conditions and thus determine J_{sc} of the double-junction device. Then, the ratio of the short-circuit current densities of the double-junction cell and the thin, optimized single-layer cell is close to $G_{\mathrm{tot}}^{\mathrm{front}}/G_{\mathrm{tot}}^{\mathrm{thin}} = 0.63$. It is thus predicted that a stack of two thin cells produces a J_{sc} that amounts to circa 63% of the value for the single-layer device. Combined with a doubled V_{oc} and an unchanged FF, an ideal double-junction device is expected to have a 26% higher efficiency than the optimized single-layer device. Based on optical modeling and measured IQE values, Eerenstein et al. have predicted a very similar increase in efficiency of 23% for an optimized PF10TBT:PCBM double-junction system. [17]

The efficiency increase that is obtained with the use of a double-junction structure can be enlarged slightly when the layer thicknesses of the subcells are chosen such that light absorption is more balanced. As indicated in Figure 6.5, combined optoelectronic simulations

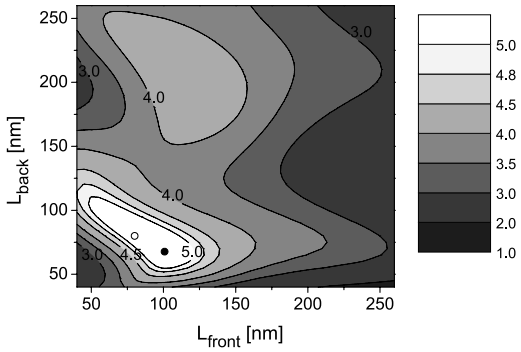

Figure 6.5: Active layer thickness dependence of the efficiency of a double-junction device as predicted by combined optoelectronic simulations. The symbols indicate the optimal combination of subcell thicknesses (filled circle) and the case of two subcells with $L_{front} = L_{back} = 80$ nm (open circle).

of double-junction devices predict that the best performance would be expected for a device with a front cell thickness front $L_{front} = 100$ nm and a back cell thickness $L_{back} = 70$ nm.* For this layer thickness combination, losses are minimized as the subcells both operate at their maximum power point. However, since a straightforward double-junction device with two 80 nm thick subcells should perform much better than a single-junction cell as well, this structure was employed in the experiments discussed below. According to the simulations the short-circuit current density of the tandem cell is slightly higher than that of the current-limiting front cell,[9,18] which causes a slight increase of the ratio of J_{sc} for the tandem and the single-layer cell to 0.65.

Comparison with experiment

Assessing the advantageous effect of a double-junction structure on the performance of a real device requires the application of the surface modification to the anode of the back cell presented in Chapter 5. To avoid a reduction of V_{oc}, an ultrathin layer of Nafion was spin coated on the middle electrode.[19] Since this interlayer is presumably only a few monolayers thick, it is not expected to affect the optical properties of the layer stack. Figure 6.6 shows the measured and simulated $J - V$ curves of single- and double-junction cells with active layers of 80 nm thickness in panels (a) and (b), respectively. At a light intensity of 0.9 sun, the experimental double-junction device delivers a J_{sc} of 34.9 A/m^2 compared to 56.0 A/m^2 for the 80 nm thick single-layer cell. The J_{sc} ratio thus amounts to 62%, which is in excellent agreement with the rationalized value of 63%. At 1.92 V the V_{oc} of the double-junction cell is very close to but slightly lower than the sum of the subcell

* The method used to predict the performance of multilayer cells is discussed in the next chapter.

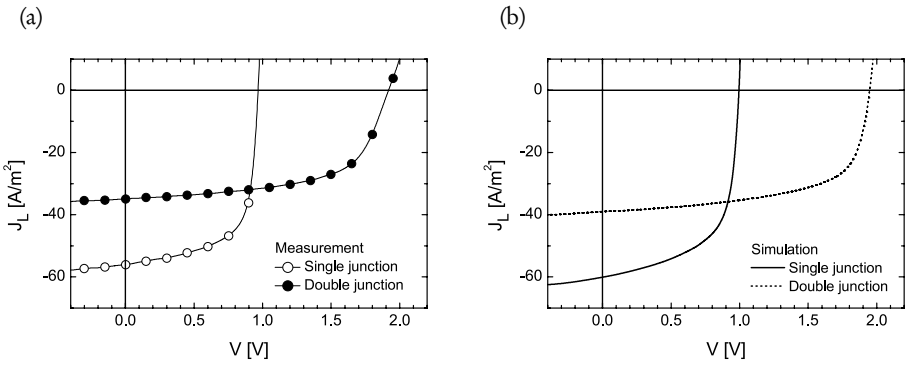

Figure 6.6: (a) Experimental and (b) calculated current density versus voltage curves of a single and a double-junction cell under illumination (experimental light intensity $\sim$ 0.9 sun). Each (sub)cell is 80 nm thick.

Table 6.2: Photovoltaic performance of the single- and double-junction cells measured at a calibrated light intensity of 0.9 sun (see Figure 6.6).

Cell type	J_{sc} [A/m^2]	V_{oc} [V]	FF	η [%]
Single junction	56.0	0.97	0.66	4.0
Double junction	34.9	1.92	0.61	4.5

voltages ($2 \times V_{oc,single} = 1.94$ V). Unfortunately, the fill factor shows a small drop as well, from 0.66 to 0.61, which is most probably caused by an additional series resistance due to the thin insulating layer between the back photoactive layer and its anode. Nevertheless, the power conversion efficiency increases with 13% from 4.0% for the optimized single-layer device to 4.5% for the double-junction device (see Table 6.2). The decoupling of optical and electronic limitations thus clearly enables an enhancement of the photovoltaic performance. The working principle is therefore generic to all polymer:fullerene systems that show optimum performance at small layer thicknesses.

6.4 Conclusions

In this chapter, we have described the photovoltaic properties of PF10TBT:PCBM solar cells with combined optoelectronic modeling to identify the processes that limit the power conversion efficiency. It was shown that 4%-efficient solar cells with an optimized layer thickness of 80 nm absorb only 48% of the photons that are available within the absorption bandwidth. Optical modeling revealed that this figure can be increased to 67% if the

PF10TBT:PCBM layer is made 210 nm thick. However, a concurrent decrease in fill factor limits the efficiency of thick cells to 3.2%. It is shown that a double-junction solar cell consisting of two optimized PF10TBT:PCBM layers absorbs photons more efficiently than thick single-layer cells, as its structure disentangles the optical and electronic limitations. Simultaneously, the subcells have the high internal quantum efficiency and fill factor associated with thin cells. Overall, the power conversion efficiency is improved from 4.0% for an optimized single-layer cell to 4.5% for the double-junction device.

6.5 Experimental

Device fabrication. ITO patterned glass substrates were thoroughly cleaned with soap water, acetone, isopropanol and a UV ozone treatment prior to application of a layer of PEDOT:PSS (Clevios VP AI4083 SG, H.C. Starck). PF10TBT (TNO, $M_w = 1.9 \times 10^5$ g/mol, PDI = 3.5) and PCBM (Solenne, > 99.5%) were used as received. Photoactive layers were spin coated under ambient conditions from hot (90 °C) chlorobenzene solutions of PF10TBT:PCBM in a 1:4 weight ratio and capped with a 1 nm LiF / 100 nm Al cathode. For the middle electrode of double-junction devices, ZnO nanoparticles with a diameter of 5 – 10 nm were synthesized in methanol via hydrolysis and condensation of zinc acetate dihydrate by KOH, as described elsewhere. [20,21] After centrifugation, the ZnO gels were dispersed in acetone, [16] followed by sonication and filtration. The acidity of PEDOT:PSS (Clevios PH500, H.C. Starck) was tuned by addition of a 1:8 dilution of 2-dimethylaminoethanol in water. [19] Nafion perfluorinated resin solution (5 wt % in a mixture of lower aliphatic alcohols and water, Aldrich) was diluted 1:20 with ethanol before spin coating at high rpm on top of *p*H-modified PEDOT:PSS layers in a nitrogen-flushed compartment under ambient atmosphere.

Characterization. Current–voltage characteristics were recorded with a Keithley 2400 SourceMeter. The results of Figure 6.1 were recorded under illumination from a Steuernagel SolarConstant 1200, producing white light with an intensity of 1.3 kW/m^2. The light intensity was determined by (a) comparison of the measured J_{sc} with the expected short-circuit current density as calculated from the convolution of the spectral responsivity curve with the AM1.5 global reference spectrum, taking into account the linear dependence of J_{sc} on light intensity and (b) the deviation of the setpoint of a multicrystalline silicon reference cell from the value determined using accurate mismatch correction. [22] The same lamp was used for the measurements of Figure 6.6a, using spectral mismatch correction ($M = 1.40$) and a GG385 filter, resulting in a light intensity equivalent to 0.9 sun. Contributions to the photocurrent from regions outside the anode/cathode overlap area were eliminated using illumination masks with slightly smaller apertures. IPCE spectra were measured at wavelengths from 400 to 1100 nm using a custom-built setup comprising a 50 W quartz tungsten halogen lamp, 28 narrow bandpass interference filters, a transimpedance amplifier and a lock-in amplifier. The spectral response was measured relative to that of a calibrated monocrystalline silicon photodiode (Newport 818-SL). Layer thickness measurements were done with a Veeco Dektak 6M or 150 profilometer. Optical absorbance was measured with a Perkin-Elmer Lambda 900 spectrophotometer.

References

[1] M. Lenes, L. J. A. Koster, V. D. Mihailetchi, and P. W. M. Blom, Appl. Phys. Lett. **88**, 243502 (2006).

[2] J. Y. Kim, S. H. Kim, H. H. Lee, K. Lee, W. L. Ma, X. Gong, and A. J. Heeger, Adv. Mater. **18**, 572 (2006).

[3] J. Gilot, I. Barbu, M. M. Wienk, and R. A. J. Janssen, Appl. Phys. Lett. **91**, 113520 (2007).

[4] B. V. Andersson, D. M. Huang, A. J. Moule, and O. Inganäs, Appl. Phys. Lett. **94**, 043302 (2009).

[5] J. Peet, J. Y. Kim, N. E. Coates, W. L. Ma, D. Moses, A. J. Heeger, and G. C. Bazan, Nat. Mater. **6**, 497 (2007).

[6] M. M. Wienk, M. Turbiez, J. Gilot, and R. A. J. Janssen, Adv. Mater. **20**, 2556 (2008).

[7] R. Kroon, M. Lenes, J. C. Hummelen, P. W. M. Blom, and B. de Boer, Polym. Rev. **48**, 531 (2008).

[8] M. M. Wienk, J. M. Kroon, W. J. H. Verhees, J. Knol, J. C. Hummelen, P. A. van Hal, and R. A. J. Janssen, Angew. Chem., Int. Ed. **42**, 3371 (2003).

[9] J. Gilot, M. M. Wienk, and R. A. J. Janssen, Adv. Mater. **22**, E67 (2010).

[10] A. Hadipour, B. de Boer, and P. W. M. Blom, Adv. Funct. Mater. **18**, 169 (2008).

[11] J. Y. Kim, K. Lee, N. E. Coates, D. Moses, T. Q. Nguyen, M. Dante, and A. J. Heeger, Science **317**, 222 (2007).

[12] D. J. D. Moet, M. Lenes, J. D. Kotlarski, S. C. Veenstra, J. Sweelssen, M. M. Koetse, B. de Boer, and P. W. M. Blom, Org. Electron. **10**, 1275 (2009).

[13] J. D. Kotlarski, P. W. M. Blom, L. J. A. Koster, M. Lenes, and L. H. Slooff, J. Appl. Phys. **103**, 084502 (2008).

[14] L. H. Slooff, S. C. Veenstra, J. M. Kroon, D. J. D. Moet, J. Sweelssen, and M. M. Koetse, Appl. Phys. Lett. **90**, 143506 (2007).

[15] L. J. A. Koster, E. C. P. Smits, V. D. Mihailetchi, and P. W. M. Blom, Phys. Rev. B **72**, 085205 (2005).

[16] J. Gilot, M. M. Wienk, and R. A. J. Janssen, Appl. Phys. Lett. **90**, 143512 (2007).

[17] W. Eerenstein, L. H. Slooff, S. C. Veenstra, and J. M. Kroon, Thin Solid Films **516**, 7188 (2008).

[18] A. Hadipour, B. de Boer, and P. W. M. Blom, Org. Electron. **9**, 617 (2008).

[19] D. J. D. Moet, P. de Bruyn, and P. W. M. Blom, Appl. Phys. Lett. **96**, 153504 (2010).

[20] C. Pacholski, A. Kornowski, and H. Weller, Angew. Chem., Int. Ed. **41**, 1188 (2002).

[21] W. J. E. Beek, M. M. Wienk, M. Kemerink, X. Yang, and R. A. J. Janssen, J. Phys. Chem. B **109**, 9505 (2005).

[22] J. M. Kroon, M. M. Wienk, W. J. H. Verhees, and J. C. Hummelen, Thin Solid Films **403**, 223 (2002).